Available online at www.sciencedirect.com
ScienceDirect
International Journal of Thermal Sciences 45 (2006) 1035–1044
International Journal of Thermal Sciences
www.elsevier.com/locate/ijts

Photothermal radiometric characterization of a thin deposit using a linear swept-frequency heat flux waveform

Jean-Luc Battaglia *, Andrzej Kusiak, Matthieu Bamford, Jean-Christophe Batsale

Laboratoire inter établissement 'TRansferts Ecoulements FLuides Energétique', UMR 8508, Ecole Nationale Supérieure d'Arts et Métiers, Esplanade des Arts et Métiers, 33405 Talence cedex, France

Received 22 August 2005; received in revised form 4 January 2006; accepted 22 February 2006

Available online 29 March 2006

Abstract

We propose a new front face thermal characterization method. The application concerns the thermal conductivity estimation of a copper oxide deposit on a tungsten carbide substrate. This method is based on the classical front face technique but in the present study the heat flux is generated as a linear swept-frequency cosine waveform. Since the thermophysical properties of the substrate are known, the thermal conductivity of the deposit is estimated from the gain values of the transfer function without measuring absolute magnitudes of the heat flux and the temperature. This approach preserves the advantages of the traditional periodic method. Additionally, the method permits performing the thermal characterization of a material from a single experiment but with much more reliability than the classical impulse method.

Keywords: Radiative photothermal experiment; Front face technique; Frequency modulation; Linear swept-frequency cosine waveform; Correlation analysis; Thermal conductivity; Thin deposit

1. Introduction

The thermal conductivity estimation of thin solid films of sub micrometric thickness such as a coating on a substrate is well treated in the literature. There exists different experimental approaches which are all based on the front face technique: the $3-\omega$ technique [1], the photothermal infrared radiometry technique [2,3] and the thermoreflectance technique are the most popular [4,5]. The front face experiment consists in heating the deposit surface and measuring the temperature rise at some or several points on the heated area. This well-known configuration is represented in Fig. 1.

Classically, the heat flux at the surface is generated by performing a periodic or an impulse photothermal waveform using a laser for example. The modulated approach (see [6] for example) consists in measuring the gain and the phase between the periodic heat flux and the temperature at each frequency of the explored domain. Nevertheless, it is required to reach the sliding behaviour, where the mean temperature value is constant, for each frequency of the explored domain. Hence, it is clear that the measurement process can be relatively time consuming according to the value of the substrate thickness, more especially considering a broad explored frequential domain. For that, many authors seek the response to a pulse of the heat flux (see [7] for example). In theory the impulse response must lead to the same result than that obtained by applying the modulated technique. Indeed, the theorical impulse response has a uniform power spectral density on the entire explored frequential domain. In practice, the impulse response is more affected by noise measurement than the modulated one. In addition, it is always seek the best compromise between the pulse duration and its magnitude. High magnitude allows measuring the impulse response with a better accuracy but, on the other hand, it can generate nonlinear phenomena at the detector as well as for the heat transfer into the sample. On the other hand, when the duration of the pulse becomes large, the power spectral density vanishes for high frequencies.

* Corresponding author. Tel.: +33 5 56 84 54 21; fax: +33 5 56 84 54 36.
E-mail address: jean-luc.battaglia@ensam.bordeaux.fr (J.-L. Battaglia).

1290-0729/$ – see front matter
doi:10.1016/j.ijthermalsci.2006.02.005

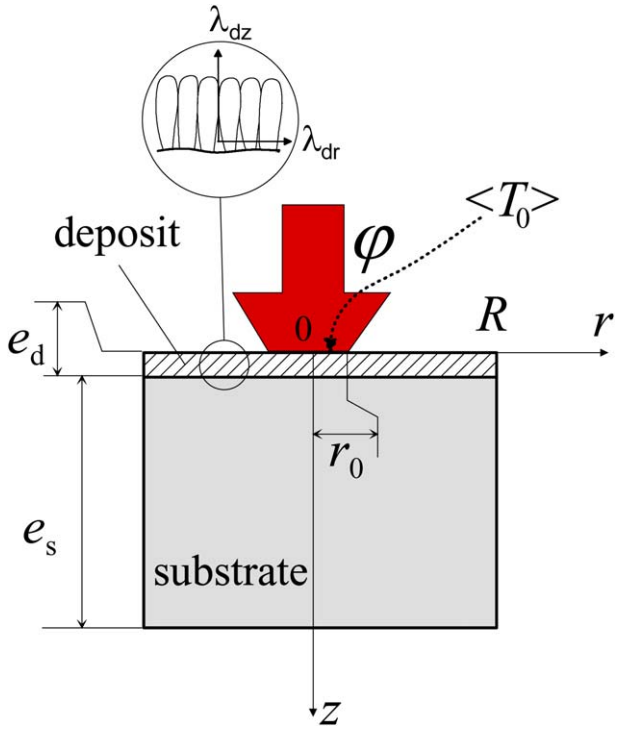

Fig. 1. Deposit thermal characterisation using the front face experiment. A transient heat flux density φ is applied on the deposit surface (over the disc of radius r_0) and one measures the average temperature $\langle T_0 \rangle$ on the heated area.

For a few years, some authors have shown the interest in using the heat flux on the form of a Pseudo Random Binary Signal (PRBS). The impulse response is then rebuilt using signal processing tools starting from transient heat flux and temperature measurements. This approach has been applied in the field of non-destructive thermal characterization [8] (detection of defects in a material for example). It has also been applied in order to identify the heat transfer model of a system in order to solve the inverse problem [9] (heat flux estimation at a boundary).

The aim of the present study is to prove that using a swept-frequency cosine heat flux waveform is certainly the more adapted waveform. We illustrate our matter on a standard configuration encountered in the thermophysical characterisation framework: the thermal conductivity estimation of a deposit on a substrate whose properties are perfectly known. The deposit is CuO, thickness 750 nm, and the substrate is tungsten carbide, thickness 1 mm. Measurements have been performed on a photothermal radiometry bench. Only the transient evolutions of the heat flux and the temperature are recorded without consideration on their absolute magnitudes. Indeed, as it will be viewed, the magnitude of the gain at the lowest frequency only depends on the thermophysical properties of the substrate. Thus, the measured gain is readjusted staring from its calculated value at this frequency. In a first stage, the swept frequency domain is defined from the sensitivity analysis of the gain versus the thermal conductivity of the deposit. Then, this thermal conductivity is identified using the modulated technique in order to define a reference value. In a second stage, the heat flux is performed on the form of a linear swept-frequency cosine signal. The gain is rebuilt using the correlation analysis which is very fast and simple. Finally the thermal conductivity of the deposit is identified from this rebuilt gain.

2. Photothermal IR radiometry experiment

The schematic view of the experimental setup is shown in Fig. 2. The heat flux is generated at the surface of the deposit using a laser diode of 808 nm wavelength and 5 W power max. The laser power is driven from the frequency function generator. Focused on the mirror by a convex lens the laser beam is redirected perpendicularly to the surface of the sample. The laser beam has a uniform profile as specified by the constructor. A very fast photodiode is used to measure the heat flux variation in order to avoid the phase lag due to the laser diode driver at high frequency. The optical thickness of absorption in the deposit depends on the wavelength of the incident laser beam. The literature gives some values of the complex refractive index of the CuO according to the wavelength (see Ref. [10]). Knowing that the refracted wave attenuates along the distance z following: $\exp(-4\pi k_\lambda z/\lambda)$, where $k = 2$ is the extinction coefficient at $\lambda = 800$ nm, it is found a thickness of absorption of approximately 32 nm to the maximum, which is not negligible behind the thickness of the deposit (750 nm). A laser with a UV wavelength would certainly be more convenient but available powers are up to now insufficient to obtain a significant temperature rise on the heated area.

The thermal response is measured using HgCdTe based photovoltaic infrared detector, cooled down to liquid nitrogen temperature (77 K). Its measurement wavelength range is 5–13 μm (see Fig. 3). The elliptical mirror, coated with bright rhodium (reflectivity 98% in the infrared wavelength band—see Fig. 3), is used to collect the emitted infrared radiation and to focus it on the sensor. The heated surface of the sample is located at the interior focal point of the mirror and the sensitive element of the detector at the exterior one, what results in a conjugate focused system. The incident laser beam is centred and aligned relatively to the focal axis of the mirror. The minimum wavelength viewed from the detector (5 μm) is greater than that of the laser (0.8 μm), what allows not disturbing the measurement with the photothermal source. The zone viewed by the detector is the image of the infrared sensitive element on the sample; it approximately corresponds to a disk with radius $r_m = 0.5$ mm. As represented in Fig. 4, the HgCdTe responsivity vanishes when the measured signal frequency is below 10 Hz and it is constant from 10 Hz up to 10 kHz. Thereby, the detector is not sensitive to the constant part of the measured signal. The signal from the detector is amplified and visualized on a digital oscilloscope together with the photodiode signal. A lock-in amplifier is used to measure the gain and the phase shift between the reference and the detector signals with respect to frequency (it is only used for a periodic heat flux). The signal from the infrared detector is exploitable up to 2 kHz. As demonstrated later, this value is sufficient to estimate the thermal conductivity of the deposit. The measurement error concerning the IR detector and the photodiode in the 10–2000 Hz frequency range were studied resulting in constant standard deviations on the entire frequency domain: 0.008 V for the sensor and 0.0075 V for the photodiode.

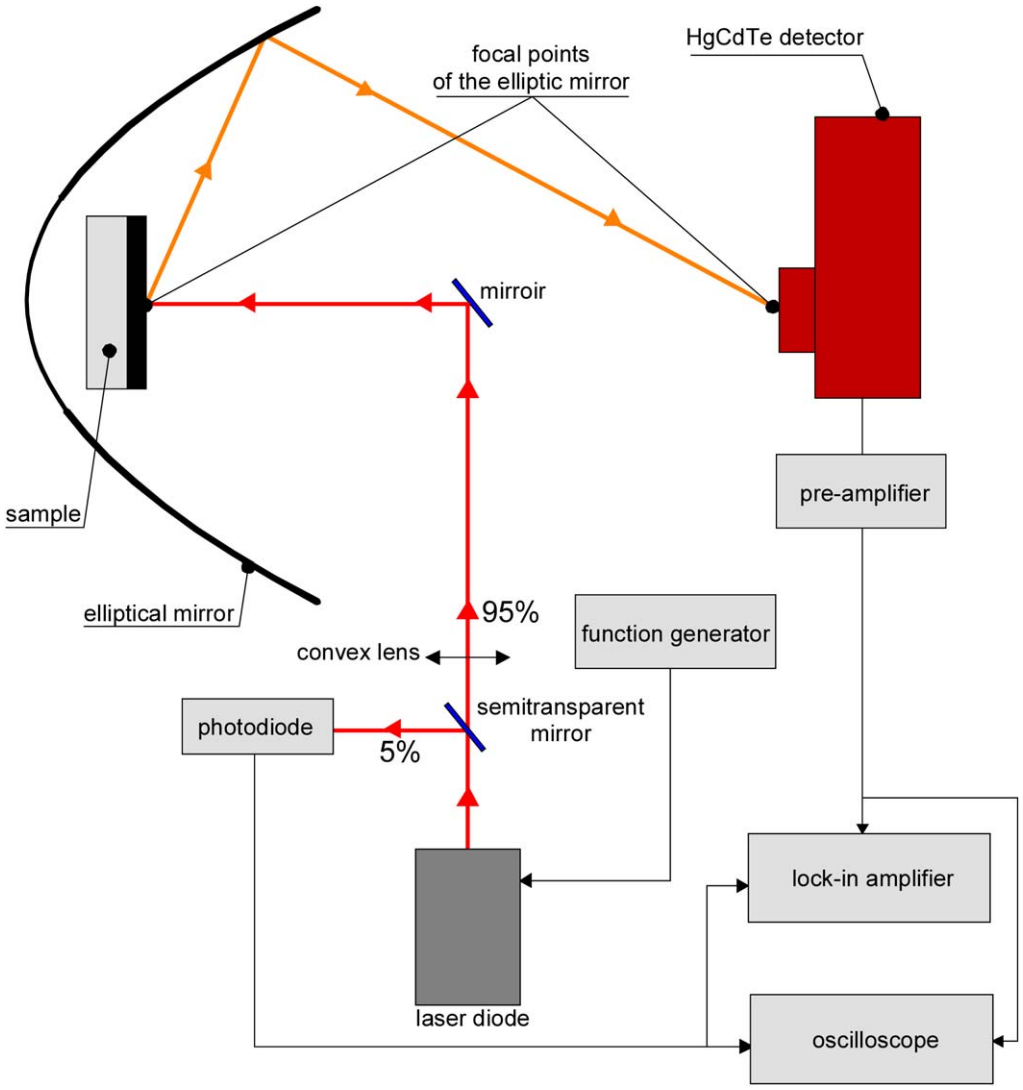

Fig. 2. Schematic view of the experimental setup.

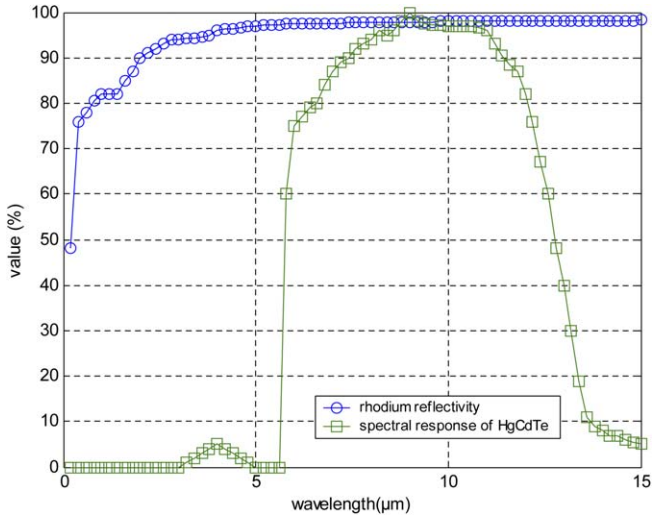

Fig. 3. Spectral response of the infrared detector and of the mirror reflectivity as a function of the wavelength.

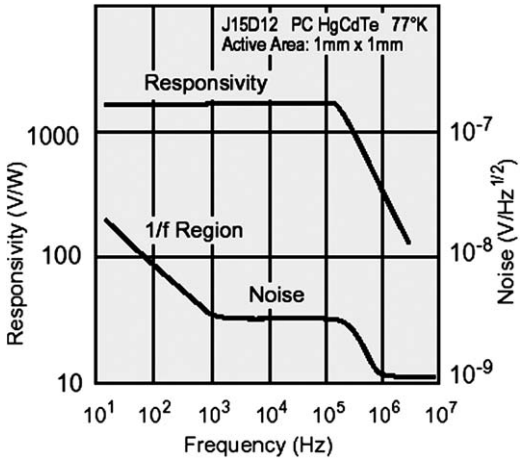

Fig. 4. HgCdTe infrared detector responsivity and noise versus frequency.

Ref. [10] gives a CuO surface emissivity close to 0.5 for $\lambda = 800$ nm but it varies according to the deposition process parameters and the surface roughness. Thereby, its exact determination involves specific experiment. However, the incident heat flux cannot easily be quantified even when using the calibration curve from the constructor. Thus, the available measurable quantities are the voltages at the HgCdTe sensor and at the photodiode.

In practice, the heat flux comprises a continuous component which it also called the offset and whose value is at least equal to the magnitude of the sinusoidal component. This offset can be also selected large enough in order to increase the detectivity of the sensor.

3. Heat transfer modelling

According to the experimental cylindrical geometry represented in Fig. 1, the temperature $T(r,z,t)$ at each point of the medium is given from the governing equations of heat transfer in the deposit and the substrate:

$$\begin{cases} (\rho C_p)_d \frac{\partial T}{\partial t} = \frac{\lambda_{dr}}{r}\frac{\partial}{\partial r}\left(r\frac{\partial T}{\partial r}\right) + \lambda_{dz}\frac{\partial^2 T}{\partial z^2}, & 0 < z < e_d \\ \frac{1}{a_s}\frac{\partial T}{\partial t} = \frac{1}{r}\frac{\partial}{\partial r}\left(r\frac{\partial T}{\partial r}\right) + \frac{\partial^2 T}{\partial z^2}, & e_d < z < e_d + e_s \\ 0 < r < R,\ t > 0 \end{cases} \quad (1)$$

λ_{dr} and λ_{dz} are the thermal conductivity of the deposit in the radial and longitudinal directions respectively, $(\rho C_p)_d$ is the volumic heat of the deposit and a_s is the thermal diffusivity of the substrate that is assumed to be isotropic.

The boundary conditions at the surface of the deposit are:

$$-\lambda_d \frac{\partial T}{\partial z} = \begin{cases} \varphi_0(r,t) + hT, & 0 < r \leqslant r_0,\ z = 0, \\ hT, & r_0 < r < R,\ z = 0, \end{cases} \quad t > 0 \quad (2)$$

h is the heat exchange coefficient and φ_0 is the heat flux density applied by the laser. The cylindrical symmetry and thermal insulation condition at the periphery lead to the following relation:

$$\frac{\partial T}{\partial r} = 0, \quad r = 0,\ r = R,\ 0 < z < e_d + e_s,\ t > 0 \quad (3)$$

Heat exchange at the interface between the substrate and the ambient is written as:

$$-\lambda_s \frac{\partial T}{\partial z} = hT, \quad 0 < r < R,\ z = e_d + e_s,\ t > 0 \quad (4)$$

The thermal contact resistance R_c at the deposit-substrate interface is defined as:

$$T_d - T_s = R_c \varphi, \quad 0 < r < R,\ z = e_d,\ t > 0 \quad (5)$$

With heat flux continuity at the interface:

$$\lambda_s \frac{\partial T_s}{\partial z} = \lambda_{dz}\frac{\partial T_d}{\partial z}, \quad 0 < r < R,\ z = e_d,\ t > 0 \quad (6)$$

Finally, the initial condition is:

$$T = 0, \quad 0 \leqslant r \leqslant R,\ 0 \leqslant z \leqslant e_d + e_s \quad (7)$$

As demonstrated see Appendix A, applying integral transforms on time and radial coordinate leads expressing the average temperature at the surface viewed by the sensor with respect to the heat flux on the following functional form (p denotes the Laplace variable and α_n the Hankel variable):

$$\langle \theta_0(p) \rangle = Z(p)F(p) \quad (8)$$

$Z(p)$ is the transfer function which is found as:

$$Z(p) = \frac{r_0^2}{R^2}\frac{\beta_0}{1 + h\beta_0} + \sum_{n=1}^{\infty} \frac{4r_0 J_1(\alpha_n r_m) J_1(\alpha_n r_0)}{\alpha_n^2 r_m R^2 J_0(\alpha_n R)^2}\frac{\beta_n}{1 + h\beta_n} \quad (9)$$

With

$$\beta_n = \frac{A_n + hB_n}{C_n + hD_n} \quad (10)$$

At low frequencies, it is obtained:

$$\begin{cases} A_n = \cosh(k_s e_s) + R_d \lambda_s k_s \sinh(k_s e_s) \\ B_n = \frac{\sinh(k_s e_s)}{\lambda_s k_s} + R_d \cosh(k_s e_s) \\ C_n = \lambda_s k_s \sinh(k_s e_s) \\ D_n = \cosh(k_s e_s) \end{cases} \quad (11)$$

With

$$k_s = \sqrt{\frac{p}{a_s} + \alpha_n^2} \quad \text{and} \quad k_d = \sqrt{\frac{(\rho C_p)_d p}{\lambda_{dz}} + \frac{\lambda_{dr}}{\lambda_{dz}}\alpha_n^2} \quad (12)$$

And

$$\alpha_n R \approx \pi\left(n + \frac{1}{4}\right) - \frac{3}{8\pi(n + \frac{1}{4})}, \quad \alpha_0 = 0 \quad (13)$$

The gain of the transfer function is defined as:

$$G(j\omega) = 20\log_{10}\left\| Z(j\omega) \right\| \quad (14)$$

Thus, the gain is the Fourier transform of the impulse response or, in other terms, it is the spectral representation of the impulse response.

In relation (11), the thermal resistance R_d includes the longitudinal thermal conductivity of the deposit as well as the thermal contact resistance R_c at the deposit-substrate interface as:

$$R_d = \frac{e_d}{\tilde{\lambda}_d} = \frac{e_d}{\lambda_{dz}} + R_c \quad (15)$$

Without loss of generality we will continue to call $\tilde{\lambda}_d$ the thermal conductivity of the deposit while keeping in mind it also appeals to the interface thermal resistance.

4. Preliminary analysis

The thermophysical properties of the substrate were measured using the hot disk technique [11] for the thermal conductivity and a differential scanning calorimeter for the specific heat. These properties are reported in Table 1 including their standard deviations. Heat exchange with the ambient is characterized by $h = 5\ \mathrm{W\,m^{-2}\,K^{-1}}$. This value has not a significant effect on the temperature with regards to the explored frequency range. Deposit thickness (750 ± 5 nm) has been measured during the pressure vaporization process and on a SEM device after deposition.

Table 1
Measured thermophysical properties of the tungsten carbide substrate (Hot Disk method)

Material	Thickness e [mm]	Diameter $2R$ [mm]	Density ρ [kg m^{-3}]	Thermal conductivity (Hot Disc) λ [W m^{-1} K^{-1}]	Specific heat (DSC) C_p [J kg^{-1} K^{-1}]
Wc-Co 9%	1 ± 0.01	16 ± 0.01	14264 ± 200	41 ± 4	206 ± 10

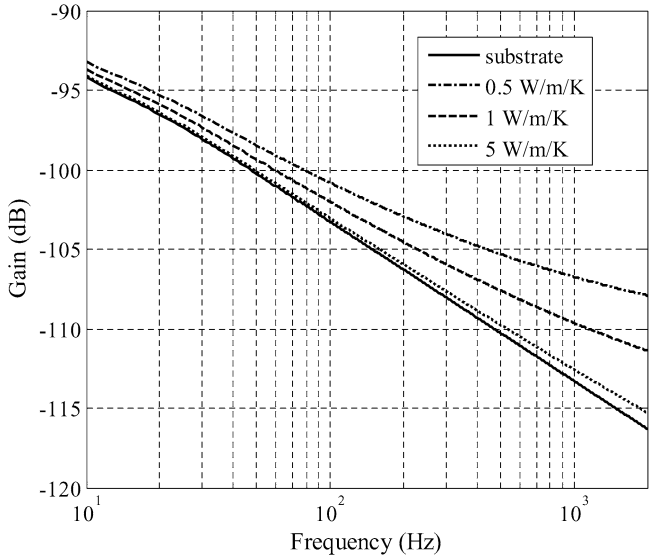

Fig. 5. Sensitivity of gain versus $\tilde{\lambda}_d$ in the [10–2000] Hz frequency range. $\lambda_s = 41\ \mathrm{W\,m^{-1}\,K^{-1}}$, $(\rho C_p)_s = 2.938 \times 10^6\ \mathrm{J\,m^{-3}\,K^{-1}}$, $e_s = 1$ mm, $(\rho C_p)_d = 2.898 \times 10^6\ \mathrm{J\,m^{-3}\,K^{-1}}$, $e_d = 0.75\ \mu$m, $r_0 = 1.5$ mm, $r_m = 0.5$ mm, $h = 5\ \mathrm{W\,m^{-2}\,K^{-1}}$.

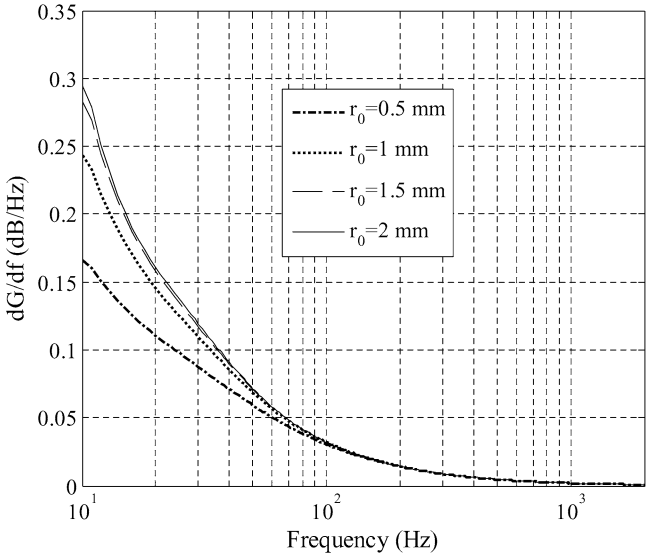

Fig. 6. Sensitivity of $\mathrm{d}G/\mathrm{d}f$ versus r_0 in the [10–2000] Hz frequency range for the uncoated sample. $\lambda_s = 41\ \mathrm{W\,m^{-1}\,K^{-1}}$, $(\rho C_p)_s = 2.938 \times 10^6\ \mathrm{J\,m^{-3}\,K^{-1}}$, $e_s = 1$ mm, $r_m = 0.5$ mm, $h = 5\ \mathrm{W\,m^{-2}\,K^{-1}}$.

The known thermal parameters (see Table 1) are used to plot the gain for different values of $\tilde{\lambda}_d$ (defined in relation (15)) in the 10–2000 Hz frequency range. As it is represented in Fig. 5, it clearly appears that this parameter can be estimated while sweeping this frequency range. It can be seen that the simulated gains for the coated and uncoated samples are almost the same at low frequencies (close to -94 dB at 10 Hz). This means that knowing the thermophysical properties of the substrate, one can adjust the value of the measured gain for the coated sample at 10 Hz. Hence, it is no longer necessary measuring absolute values of the temperature and the heat flux to identify the deposit thermal conductivity. Thus, as specified previously, the measured gain is readjusted staring from its simulated value at 10 Hz that is equal to -94 dB.

Finally, the laser beam radius r_0 on the deposit cannot be measured easily. Nevertheless, it can be identified from the derivative of the gain vs. frequency as represented in Fig. 6.

5. Linear swept-frequency heat flux waveform

We assume a heat flux on the form of a linear swept-frequency cosine signal:

$$\varphi_0(t) = \sin\bigl(2\pi f(t)t\bigr) \tag{16}$$

The frequency varies linearly with time as:

$$f(t) = f_0 + \frac{f_1 - f_0}{t_1}t, \quad 0 \leqslant t \leqslant t_1 \tag{17}$$

f_0 is the instantaneous frequency at time 0, and f_1 is the instantaneous frequency at time t_1.

Based on the linearity assumption, the measured temperature $\langle y_0(t)\rangle$ is related to the heat flux $\varphi_0(t)$ from the convolution product:

$$\bigl\langle y_0(t)\bigr\rangle = \int_0^\infty h_0(t-\tau)\varphi_0(\tau)\,\mathrm{d}\tau + e(t) \tag{18}$$

$h_0(t)$ is the impulse response and $e(t)$ denotes the measurement error.

Now, let us multiply the two members of this equality by $\varphi_0(t-\tau)$ and integrate from $t = 0$ to infinity. It is then obtained:

$$\int_0^\infty \bigl\langle y_0(t)\bigr\rangle\varphi_0(t-\tau)\,\mathrm{d}t = \int_0^\infty h_0(t-\tau)\left(\int_0^\infty \varphi_0(\tau)\varphi_0(t-\tau)\,\mathrm{d}t\right)\mathrm{d}\tau + \int_0^\infty \varphi_0(t-\tau)e(t)\,\mathrm{d}t \tag{19}$$

One recognizes the cross and auto correlation functions, $C_{y_0\varphi}(\tau)$, $C_{\varphi e}(\tau)$ and $C_{\varphi\varphi}(\tau)$. Relation (19) is thus written on the following form:

$$C_{y_0\varphi}(\tau) = \int_0^\infty h_0(t-\tau)C_{\varphi\varphi}(\tau)\,\mathrm{d}\tau + C_{\varphi e}(\tau) \tag{20}$$

By choosing the heat flux $\varphi_0(t)$ as a white noise lead to:

$$C_{\varphi\varphi}(\tau) = \delta(\tau) \tag{21}$$

Finally, if it is admitted that the noise measurement is not correlated to the heat flux ($C_{e\varphi} = 0$), relation (20) is summarized to:

$$C_{y_0\varphi}(\tau) = h_0(\tau) \tag{22}$$

One sees that the impulse response is equal to the cross correlation function between the temperature of the sensor and the heat flux. This approach is very sensitive to noise measurement magnitude, so one would rather use the power spectral density (PSD) instead of the correlation function. In practice, it consists in applying the Fourier transform on the cross correlation and auto correlation functions, i.e.:

$$\begin{aligned}\mathrm{FFT}\big[C_{y_0\varphi}(\tau)\big] &= \mathrm{FFT}\left[\int_0^\infty h_0(t-\tau)C_{\varphi\varphi}(\tau)\,\mathrm{d}\tau\right] \\ &= Y_0(f)\Phi_0(f) = S_{y_0\varphi}(f)\end{aligned} \tag{23}$$

and

$$\begin{aligned}\mathrm{FFT}\big[C_{\varphi\varphi}(\tau)\big] &= \mathrm{FFT}\left[\int_0^\infty \varphi_0(t-\tau)\varphi_0(\tau)\,\mathrm{d}\tau\right] \\ &= \Phi_0(f)^2 = S_{\varphi\varphi}(f)\end{aligned} \tag{24}$$

$Y_0(f)$ and $\Phi_0(f)$ are the Fourier transforms of the temperature and the heat flux respectively as well as $S_{\varphi\varphi}(f)$ and $S_{y_0\varphi}(f)$ are the auto and cross PSD. Then, by applying the Fourier transform on relation (20) it is immediately obtained:

$$S_{y_0\varphi}(f) = H(f)S_{\varphi\varphi}(f) + S_{\varphi e}(f) \tag{25}$$

Finally, assuming that the noise measurement is not correlated with the heat flux ($S_{\varphi e}(f) = 0$), the expression of the transfer function is:

$$H(f) = \frac{S_{y_0\varphi}(f)}{S_{\varphi\varphi}(f)} \tag{26}$$

Since the length of the experiment is set to a fixed value τ, the real input signal is:

$$\varphi_\Pi(t) = \varphi_0(t)\Pi_\tau(t) \tag{27}$$

In this relation, $\Pi_\tau(t) = 1$ when $0 \leqslant t \leqslant \tau$ and 0 elsewhere. Then applying the Fourier transform on the heat flux leads to:

$$\Phi_\Pi(f) = \Phi_0(f) \cdot \left(\tau\frac{\sin(\pi\tau f)}{\pi\tau f}\right) \tag{28}$$

It appears that the Fourier transform of the heat flux is convoluted by the sinus cardinal function. Usually, the heat flux is pre-windowed by a specific function $g_\tau(t)$ which decreases the influence of the function $\Pi_\tau(t)$ as:

$$\varphi_\Pi(t) = \varphi_0(t)g_\tau(t) \tag{29}$$

For example, it is often used of the Hanning window [12,13] defined by:

$$g_\tau(t) = 0.5\left(1 - \cos\left(\frac{2\pi t}{\tau}\right)\right) \tag{30}$$

It is used an improved estimation of $S_{y_0\varphi}(f)$ and $S_{\varphi\varphi}(f)$ proposed by Welch [14]. The method consists in dividing the time series data into possible overlapping segments, computing the auto and cross power spectral densities and averaging the estimates.

6. Experimental results

6.1. Periodic heat flux

The heat flux has a periodic waveform. The gain is measured for the uncoated sample in the $f = [10\text{–}30]$ Hz frequency range. Since the thermophysical properties of the tungsten carbide are known, the laser beam radius r_0 on the sample is identified by minimizing the gap between the measured and simulated value of the derivative of the gain versus frequency: $\mathrm{d}G/\mathrm{d}f$. The minimization algorithm is a subspace trust region method and is based on the interior-reflective Newton method described in [15,16]. Each iteration involves the solution of a large linear system using the method of preconditioned conjugate gradients (PCG). The measured gain and the simulated one using the identified value of the laser beam radius $r_0 = 1.5$ mm are plotted in Fig. 7.

In the second step, the gain is measured for the coated sample in the $f = [10\text{–}2000]$ Hz frequency range. The longitudinal

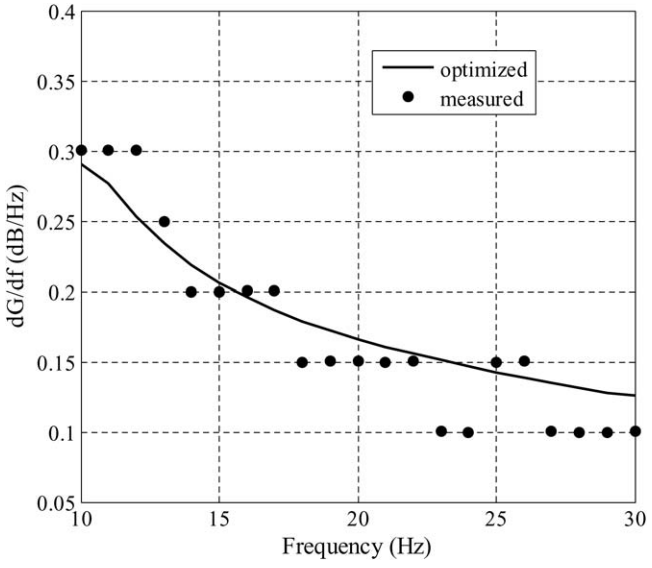

Fig. 7. Comparison between experimental and simulated values of $\mathrm{d}G/\mathrm{d}f$ for the uncoated sample. Simulated values are obtained with the identified value of $r_0 = 1.5$ mm.

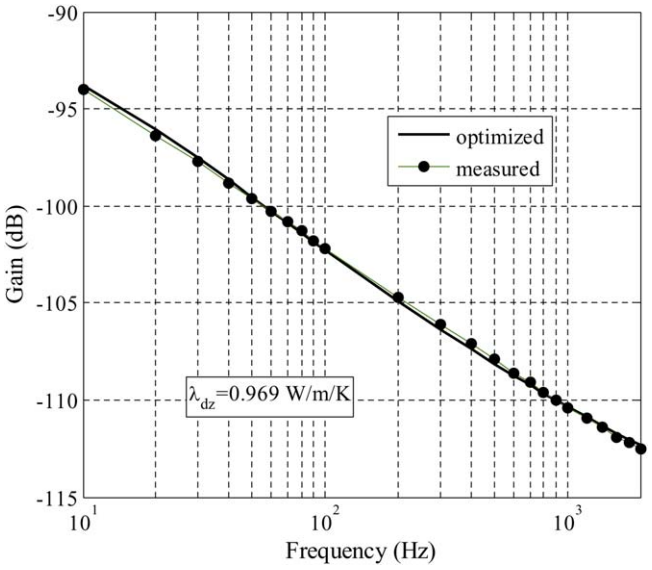

Fig. 8. Comparison between the measured gain and the simulated one with $\tilde{\lambda}_d = 0.97\ \mathrm{W m^{-1} K^{-1}}$.

thermal conductivity of the deposit is identified by minimizing the quadratic gap between the theorical and experimental values of the gain. It is found $\tilde{\lambda}_d = 0.97\ \mathrm{W m^{-1} K^{-1}}$ which constitutes the reference value. The comparison between the measured gain and the fitted one, with this identified value, is represented in Fig. 8.

6.2. Linear-swept frequency heat flux

The heat flux has now a linear swept frequency waveform as described by relation (16) with $f_0 = 10$ Hz and $f_1 = 3000$ Hz. The measured signal from the detector is shown in Fig. 9 when the sliding behaviour is reached (approximately 10 sec.). Acquisition time has been set to $\Delta t = 2 \times 10^{-4}$ sec. This means that the sampling rate is approximately tenth larger that the maximum value of the swept domain. First, we can observe that the noise measurement is weak and constant for all times. This means that the response is exploitable for the entire explored frequency domain. As shown in Fig. 10, the power spectral density of the heat flux is quasi-constant all over the frequency range of interest which is [100–2000] Hz. In other words, the heat flux waveform has the same features as those of a white noise in this domain.

Using the Welch technique described below, with 512 samples per time interval and 256 overlapping samples, it is obtained the gain plotted in Fig. 11. The measured gain obtained previously by using the modulated method is also plotted in the same figure. It is seen that the agreement between the two quantities is very satisfying. Using the rebuilt gain, it is found that the identified thermal conductivity of the deposit is equal to $\tilde{\lambda}_d = 1.01\ \mathrm{W m^{-1} K^{-1}}$ which is very close to the reference value. The comparison between the rebuilt gain and the simulated one using this identified value is plotted in Fig. 12.

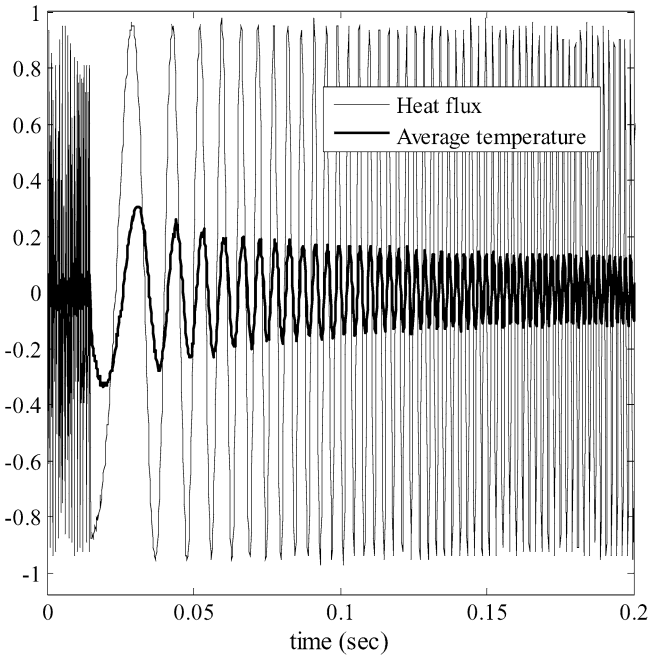

Fig. 9. Response to a linear swept-frequency cosine signal. The frequency varies linearly from 10 Hz to 3000 Hz.

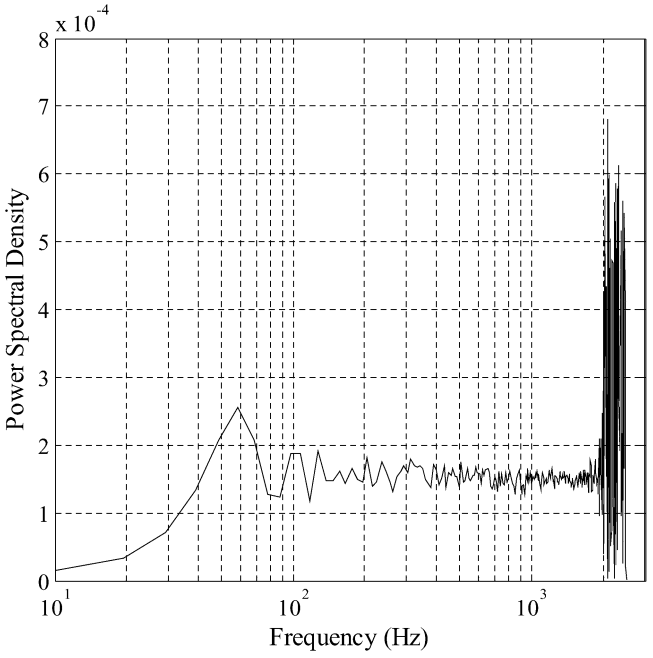

Fig. 10. Power spectral density of the generated linear swept-frequency cosine signal.

7. Discussion

The swept-frequency cosine heat flux waveform has two major interesting features. The first is that the offset must be easily removed from the experimental heat flux in order to fully satisfy the relation (21). The second feature is that the explored frequential domain, defined from the sensitivity analysis, is perfectly swept. It has been proved by representing the power spectral density of the heat flux in Fig. 11. This feature is also

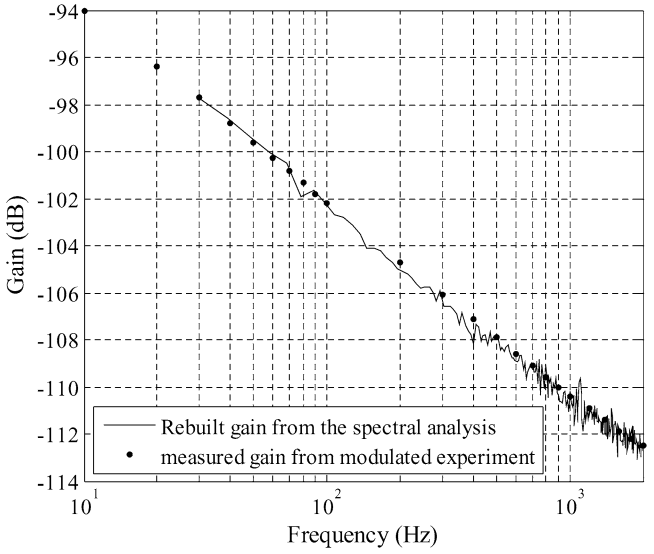

Fig. 11. Comparison between the rebuilt gain, using the spectral analysis method, and that obtained from the modulated technique.

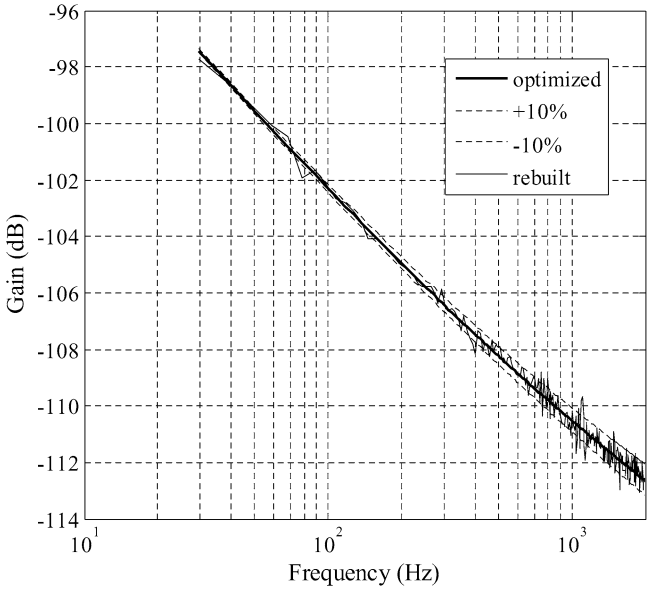

Fig. 12. Comparison between the rebuilt gain and the simulated one with $\tilde{\lambda}_d = 1.01\ \mathrm{W\,m^{-1}\,K^{-1}}$.

highlighted in Fig. 13 by plotting the heat flux spectrum, in a time-frequency representation. Furthermore, the use of auto and cross power spectral density functions allows defining the so-called coherence function as:

$$C_{y_0\varphi}(f) = \frac{|S_{y_0\varphi}(f)|^2}{S_{y_0y_0}(f)S_{\varphi\varphi}(f)} \tag{31}$$

This function can be viewed as the correlation coefficient between the temperature and the heat flux and lies between 0 and 1. If it is 1 at a certain frequency, then there is perfect correlation between the two signals at this frequency. In other words, there is consequently no noise interfering at this frequency, which is confirmed from relation (25) what lead to:

$$S_{\varphi e}(f) = S_{y_0y_0}(f)\big(1 - C_{y_0\varphi}(f)\big) \tag{32}$$

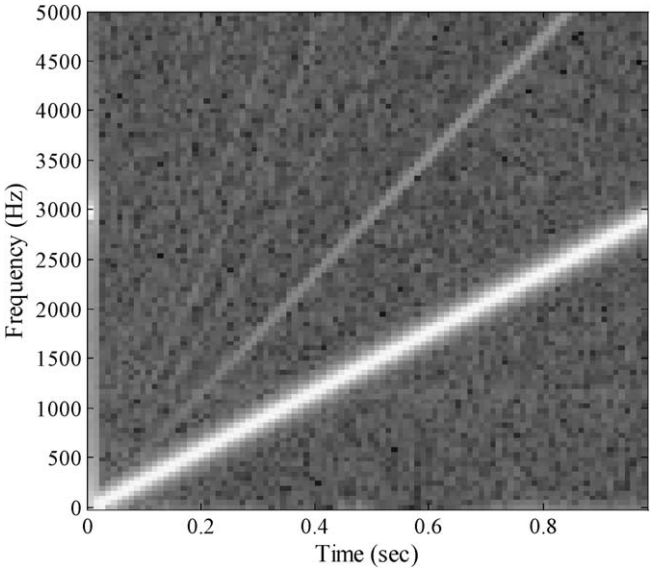

Fig. 13. Measured linear swept-frequency cosine heat flux spectrum.

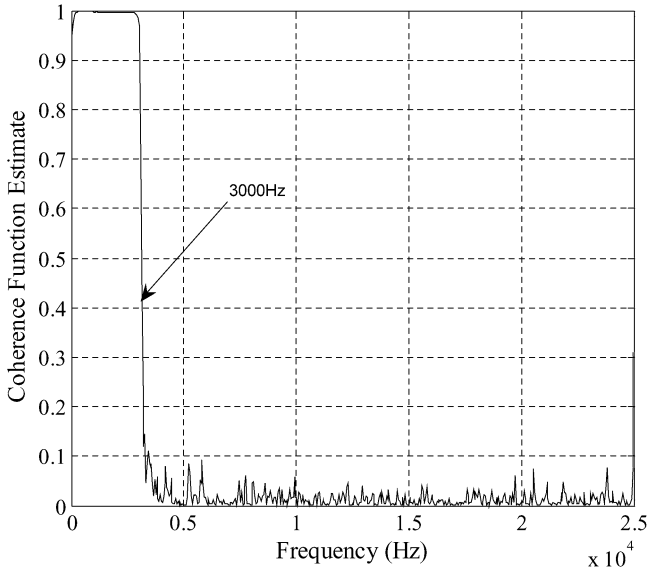

Fig. 14. Coherence function calculated from experimental data represented in Fig. 10.

The coherence function is represented in Fig. 14 from experimental data plotted in Fig. 9. One sees clearly that the heat flux and the temperature are perfectly correlated on the [10–3000] Hz frequency range and uncorrelated elsewhere. This explains why the noise measurement has a negligible effect for each swept frequency on the rebuilt gain as shown in Fig. 11.

8. Conclusion

The preceding results show that the response to a linear swept-frequency cosine heat flux permits to identify the thermal conductivity of a material with accuracy comparable to that obtained with the traditional modulated technique. The interest is first of all to preserve the advantages of the mod-

ulated technique, namely the use of a small magnitude heat flux which preserves the linearity assumption as well at the level of the detector as for the heat transfer in material. A constant power spectral density is obtained on the entire swept frequential domain what confirms that the measurement noise has approximately the same influence for each swept frequency. The additional interest of this approach is that a single experiment is required in order to characterise the material, like for the impulse method. This method is well-suited for the thermal characterisation of large-sized materials, requiring a relatively long time to reach the stationary behaviour.

Appendix A

Applying the Laplace transform, versus the time variable, on the temperature and the heat flux density leads to:

$$\theta(r,z,p)=\int_0^\infty T(r,z,t)e^{-pt}\,\mathrm{d}t,$$

$$\psi(r,p)=\int_0^\infty \varphi(r,t)e^{-pt}\,\mathrm{d}t \tag{A.1}$$

Therefore, relations (1)–(7) become:

$$\begin{cases}(\rho C_p)_d s\theta=\frac{\lambda_{\mathrm{d}r}}{r}\frac{\partial}{\partial r}\left(r\frac{\partial\theta}{\partial r}\right)+\lambda_{\mathrm{d}z}\frac{\partial^2\theta}{\partial z^2}, & 0<z<e_d\\ \frac{s}{a_s}\theta=\frac{1}{r}\frac{\partial}{\partial r}\left(r\frac{\partial\theta}{\partial r}\right)+\frac{\partial^2\theta}{\partial z^2}, & e_d<z<e_d+e_s\\ 0<r<R\end{cases} \tag{A.2}$$

$$-\lambda_d\frac{\partial\theta}{\partial z}=\begin{cases}\psi_0+h\theta, & 0<r\leqslant r_0,\ z=0\\ h\theta, & r_0<r<R,\ z=0\end{cases} \tag{A.3}$$

$$\frac{\partial\theta}{\partial r}=0,\quad r=0,\ r=R,\ 0<z<e_d+e_s \tag{A.4}$$

$$-\lambda_s\frac{\partial\theta}{\partial z}=h\theta,\quad 0<r<R,\ z=e_d+e_s \tag{A.5}$$

$$\theta_d-\theta_s=R_c\psi,\quad 0<r<R,\ z=e_d \tag{A.6}$$

$$\lambda_s\frac{\partial\theta_s}{\partial z}=\lambda_{\mathrm{d}z}\frac{\partial\theta_d}{\partial z},\quad 0<r<R,\ z=e_d \tag{A.7}$$

According to the cylindrical symmetry, one can apply the Hankel transform on the temperature and the heat flux density, versus the radial coordinate, as:

$$\bar\theta(\alpha,z,p)=\int_0^R\theta(r,z,p)rJ_0(\alpha r)\,\mathrm{d}r,$$

$$\overline{\psi}(\alpha,p)=\int_0^R\psi(r,p)rJ_0(\alpha r)\,\mathrm{d}r \tag{A.8}$$

Thus, relations (A.1)–(A.7) become:

$$\begin{cases}(\rho C_p)_d p\bar\theta=-\alpha^2\lambda_{\mathrm{d}r}\bar\theta+\lambda_{\mathrm{d}z}\frac{\mathrm{d}^2\bar\theta}{\mathrm{d}z^2}, & 0<z<e_d\\ \frac{p}{a_s}\bar\theta=-\alpha^2\bar\theta+\frac{\mathrm{d}^2\bar\theta}{\mathrm{d}z^2}, & e_d<z<e_d+e_s\end{cases} \tag{A.9}$$

$$-\lambda_d\frac{\partial\bar\theta}{\partial z}=\overline{\psi_0}(\alpha,p)+h\bar\theta,\quad z=0 \tag{A.10}$$

$$J_1(\alpha_n R)=0,\quad 0<z<e_d+e_s \tag{A.11}$$

$$-\lambda_s\frac{\partial\bar\theta}{\partial z}=h\bar\theta,\quad z=e_d+e_s \tag{A.12}$$

$$\overline{\theta_d}-\overline{\theta_s}=R_c\overline{\psi},\quad z=e_d \tag{A.13}$$

$$\lambda_s\frac{\partial\overline{\theta_s}}{\partial z}=\lambda_{\mathrm{d}z}\frac{\partial\overline{\theta_d}}{\partial z},\quad 0<r<R,\ z=e_d \tag{A.14}$$

Relation (A.11) is a transcendental equation whose solutions are approximately:

$$\alpha_n R\approx\pi\left(n+\frac{1}{4}\right)-\frac{3}{8\pi(n+\frac{1}{4})},\quad \alpha_0=0 \tag{A.15}$$

It has been shown in the previous section that the laser beam has a uniform profile:

$$\varphi_0(r,t)=\Pi_{r_0}f(t) \tag{A.16}$$

Applying respectively the Laplace and Hankel transforms on relation (A.16) lead to:

$$\overline{\psi}_0(\alpha,p)=\frac{r_0}{\alpha_n}J_1(\alpha_n r_0)F(p) \tag{A.17}$$

The solution of Eq. (A.9) is on the form:

$$\bar\theta_i(\alpha,z,p)=A_1e^{k_iz}+A_2e^{-k_iz},\quad i=d,s \tag{A.18}$$

Where A_1 and A_2 (for s and d) would be determined from conditions (A.10), (A.12), (A.13) and (A.14), and:

$$k_s=\sqrt{\frac{p}{a_s}+\alpha_n^2}\quad\text{and}\quad k_d=\sqrt{\frac{(\rho C_p)_d p}{\lambda_{\mathrm{d}z}}+\frac{\lambda_{\mathrm{d}r}}{\lambda_{\mathrm{d}z}}\alpha_n^2} \tag{A.19}$$

Taking $z=0$ in relation (A.18), one obtain the expression of the transfer function that expresses the transformed temperature at the heated surface according to the transformed heat flux as:

$$\frac{\overline{\theta_0}}{\overline{\psi_0}}=\frac{\beta_n}{1+h\beta_n} \tag{A.20}$$

With

$$\beta_n=\frac{A_n+hB_n}{C_n+hD_n} \tag{A.21}$$

And

$$\begin{cases}A_n=\cosh(k_de_d)\cosh(k_se_s)\\ \qquad+\left(\cosh(k_de_d)R_c+\frac{\sinh(k_de_d)}{\lambda_dk_d}\right)\lambda_sk_s\sinh(k_se_s)\\ B_n=\frac{\sinh(k_se_s)}{\lambda_sk_s}\cosh(k_de_d)\\ \qquad+\left(\cosh(k_de_d)R_c+\frac{\sinh(k_de_d)}{\lambda_dk_d}\right)\cosh(k_se_s)\\ C_n=\lambda_dk_d\sinh(k_de_d)\cosh(k_se_s)\\ \qquad+(\lambda_dk_d\sinh(k_de_d)R_c+\cosh(k_de_d))\lambda_sk_s\sinh(k_se_s)\\ D_n=(\lambda_dk_d\sinh(k_de_d)R_c+\cosh(k_de_d))\cosh(k_se_s)\\ \qquad+\frac{\lambda_dk_d}{\lambda_sk_s}\sinh(k_de_d)\sinh(k_se_s)\end{cases} \tag{A.22}$$

At low heat flux frequencies, $f\ll a_d/e_d^2$, the deposit is viewed as a thermal resistance and the transfer function can be largely

simplified given that parameters A_n, B_n, C_n and D_n of relation (A.22) become:

$$\begin{cases} A_n = \cosh(k_s e_s) + R_d \lambda_s k_s \sinh(k_s e_s) \\ B_n = \frac{\sinh(k_s e_s)}{\lambda_s k_s} + R_d \cosh(k_s e_s) \\ C_n = \lambda_s k_s \sinh(k_s e_s) \\ D_n = \cosh(k_s e_s) \end{cases} \tag{A.23}$$

Applying the inverse Hankel transform on relation (A.20) lead to:

$$\theta_0(r, p) = \sum_{n=0}^{\infty} \frac{2J_0(\alpha_n r) r_0 J_1(\alpha_n r_0)}{R^2 \alpha_n J_0(\alpha_n R)^2} \frac{\beta_n}{1 + h\beta_n} F(p) \tag{A.24}$$

The average temperature on the measurement area is:

$$\langle \theta_0(p) \rangle = \frac{2}{r_m^2} \int_0^{r_m} \theta_0(r, p) r \, \mathrm{d}r \tag{A.25}$$

With respect to relation (A.24), one obtains an analytical expression of the average temperature on the measurement area as:

$$\langle \theta_0(p) \rangle = \left(\frac{r_0^2}{R^2} \frac{\beta_0}{1 + h\beta_0} + \sum_{n=1}^{\infty} \frac{4 r_0 J_1(\alpha_n r_m) J_1(\alpha_n r_0)}{\alpha_n^2 r_m R^2 J_0(\alpha_n R)^2} \frac{\beta_n}{1 + h\beta_n} \right) F(p) \tag{A.26}$$

In practice series in relation (A.26) is calculated with 100 terms.

References

[1] D.G. Cahill, A. Bullen, S.-M. Lee, Interface thermal conductance and the thermal conductivity of multilayer thin films, High Temperatures—High Pressures 32 (2000) 134–142.

[2] B.K. Bein, J. Bolte, D. Dietzel, A. Haj Daoud, G. Kalus, F. Macedo, A. Linnenbrüger, H. Bosse, J. Pelzl, Photothermal characterization of amorphous thin films, Surface and Coatings Technology 116–119 (1999) 147–154.

[3] G. Langer, J. Hartmann, M. Reichling, Thermal conductivity of thin metallic films measured by photothermal profile analysis, Rev. Sci. Instrum. 68 (3) (1997) 1510–1513.

[4] S. Orain, Y. Scudeller, T. Brousse, Thermal conductivity of ZrO_2 thin films, International Journal of Thermal Science 39 (2000) 537–543.

[5] S. Dilhaire, S. Grauby, W. Claeys, J.-Ch. Batsale, Thermal parameters identification of micrometric layers of microelectronic devices by thermoreflectance microscopy, Microelectronics Journal 35 (2004) 811–816.

[6] C. Gervaise, C. Nouals, J.J. Serra, Estimation des propriétés thermiques à l'échelle millimétriques par méthodes périodiques : résolution du problème direct et du problème inverse, International Journal of Thermal Science 39 (2000) 422–432.

[7] O. Faugeroux, B. Claudet, S. Bénet, J.J. Serra, D. Boisson, Caractérisation thermophysique de revêtements par méthode photothermique impulsionnelle en face avant, International Journal of Thermal Science 43 (2004) 383–401.

[8] J.-L. Bodnar, B. Lannoy, L. Durville, Radiométrie photothermique sous excitation aléatoire par analyses corrélatoire et paramétrique, Congrès de la Société Française de Thermiciens (1996) 637–642.

[9] A. Kusiak, J.-L. Battaglia, R. Marshall, Influence of CrN coating in wood machining from heat flux estimation in the tool, International Journal of Thermal Sciences 44 (2005) 289–301.

[10] H. Wieder, A.W. Czanderna, Optical properties of copper oxide films, Journal of Applied Physics 37 (1) (1966) 184–187.

[11] M. Gustavsson, E. Karawacki, S.E. Gustafsson, Thermal conductivity, thermal diffusivity and specific heat of thin samples from transient measurements with hot disk sensors, Rev. Sci. Instrum. 65 (1994) 3856–3859.

[12] S.M. Kay, Modern Spectral Estimation, Prentice-Hall, Englewood Cliffs, NJ, 1988.

[13] P. Stoïca, R. Moses, Introduction to Spectral Analysis, Prentice-Hall, Upper Saddle River, NJ, 1997.

[14] P.D. Welch, The use of fast Fourier transform for the estimation of power spectra: a method based on time averaging over short, modified periodograms, IEEE Trans. Audio Electroacoust. AU-15 (June 1967) 70–73.

[15] T.F. Coleman, Y. Li, An interior, trust region approach for nonlinear minimization subject to bounds, SIAM Journal on Optimization 6 (1996) 418–445.

[16] T.F. Coleman, Y. Li, On the convergence of reflective Newton methods for large-scale nonlinear minimization subject to bounds, Mathematical Programming 67 (2) (1994) 189–224.